0022-3565/08/3263-783–791$20.00
THE JOURNAL OF PHARMACOLOGY AND EXPERIMENTAL THERAPEUTICS
JPET 326:783–791, 2008

Vol. 326, No. 3
140913/3379173
Printed in U.S.A.

Ligand-Specific Contribution of the N Terminus and E2-Loop to Pharmacological Properties of the Histamine H_1-Receptor

Andrea Straßer, Hans-Joachim Wittmann, and Roland Seifert

Departments of Pharmaceutical/Medicinal Chemistry I (A.S.) and Pharmacology and Toxicology (R.S.), School of Pharmacy, University of Regensburg, Regensburg, Germany; and Faculty of Chemistry and Pharmacy, University of Regensburg, Regensburg, Germany (H.-J.W.)

Received May 7, 2008; accepted June 23, 2008

ABSTRACT

There are species differences between human histamine H_1 receptor (hH_1R) and guinea pig (gp) histamine H_1 receptor (gpH_1R) for phenylhistamines and histaprodifens. Several studies showed participation of the second extracellular loop (E2-loop) in ligand binding for some G protein-coupled receptors (GPCRs). Because there are large species differences in the amino acid sequence between hH_1R and gpH_1R for the N terminus and E2-loop, we generated chimeric hH_1Rs with gp E2-loop ($h_{gpE2}H_1R$) and gp N terminus and gp E2-loop ($h_{gpNgpE2}H_1R$). hH_1R, gpH_1R, and chimeras were expressed in Sf9 insect cells. [^{3}H]Mepyramine binding assays and steady-state GTPase assays were performed. In the series $hH_1R > h_{gpE2}H_1R > h_{gpNgpE2}H_1R$, we observed a significant decrease in potency of histamine **1** in the GTPase assay. For phenoprodifen **5** and the chiral phenoprodifens **6R** and **6S,** a significant decrease in affinity and potency was found in the series $hH_1R > h_{gpE2}H_1R > h_{gpNgpE2}H_1R$. In addition, we constructed new active-state H_1R models based on the crystal structure of the human β_2-adrenergic receptor ($h\beta_2AR$). Compared with the H_1R active-state models based on the crystal structure of bovine rhodopsin, the E2-loop differs in its contact to the ligand bound in the binding pocket. In the bovine rhodopsin-based model, the backbone carbonyl of Lys187 (gpH_1R) interacts with large histaprodifens in the binding pocket, but in the $h\beta_2AR$-based model, Lys187 (gpH_1R) is located distantly from the binding pocket. In conclusion, the differences in N terminus and E2-loop between hH_1R and gpH_1R exert an influence on affinity and/or potency for histamine and phenoprodifens **5**, **6R,** and **6S**.

G protein-coupled receptors (GPCRs) represent the largest class of cell-surface receptors, which consist of seven transmembrane helices that are connected by three extracellular and three intracellular loops (Kristiansen, 2004). The histamine H_1 receptor (H_1R) is a biogenic amine receptor that belongs to class I of the GPCRs (Foord et al., 2005), and it interacts with G_q proteins to activate phospholipase C (Hill et al., 1997).

In histaprodifens (Fig. 1), identified as potent H_1R agonists at the guinea pig (gp) ileum (Elz et al., 2000; Menghin et al., 2003), a 3,3-diphenylpropyl moiety is combined with a 2-substituted histamine. A pharmacological characterization of histaprodifens at the human H_1R (hH_1R) and guinea pig H_1R (gpH_1R) showed significant species differences (Seifert et al., 2003; Straßer et al., 2008). Several amino acids are involved in histamine binding: $Asp^{3.32}$ (Ohta et al., 1994; Nonaka et al., 1998), $Lys^{5.39}$ (Leurs et al., 1995; Bruysters et al., 2004; Jongejan and Leurs 2005), $Thr^{5.42}$ and $Asn^{5.46}$ (Leurs at al., 1994; Ohta et al., 1994), and $Phe^{6.55}$ (Bruysters et al., 2004). The amino acid side chains $Trp^{4.56}$, $Lys^{5.39}$, $Phe^{6.52}$, and $Phe^{6.5}$ were found to interact with H_1R antagonists (Wieland et al., 1999; Gillard et al., 2002).

$Asn^{2.61}$ acts as a selectivity switch between hH_1R and gpH_1R for suprahistaprodifen and dimeric histaprodifen (Bruysters et al., 2005). However, pharmacological analysis of suprahistaprodifen and dimeric histaprodifen at the bovine H_1R and the rat H_1R (Straßer et al., 2008) showed that the amino acid in position 2.61 cannot be exclusively responsible for the observed species differences.

Molecular modeling studies of dimeric histaprodifen in the binding pocket of the gpH_1R suggest that the second extracellular loop (E2-loop) is in close contact to dimeric hista-

This work was supported by the Research Training Program (Graduiertenkolleg) GRK760 "Medicinal Chemistry: Molecular Recognition–Ligand-Receptor Interactions" of the Deutsche Forschungsgemeinschaft.

Article, publication date, and citation information can be found at http://jpet.aspetjournals.org.

doi:10.1124/jpet.108.140913.

ABBREVIATIONS: GPCR, G protein-coupled receptor; H_1R, histamine H_1 receptor; gp, guinea pig; hH_1R, human H_1R; gpH_1R, guinea pig H_1R; E2-loop, second extracellular loop; $h_{gpE2}H_1R$, hH_1R with gp E2-loop; $h_{gpNgpE2}H_1R$, hH_1R with gp N terminus and gp E2-loop; RGS4, regulator of G protein signaling 4; h, human; TM, transmembrane domain; S, signal peptide; F, FLAG epitope; PCR, polymerase chain reaction; DMSO, dimethyl sulfoxide; $h\beta_2AR$, human β_2-adrenergic receptor; MD, molecular dynamics; [^{3}H]MEP, mepyramine; Cpd, compound; HA, histamine.

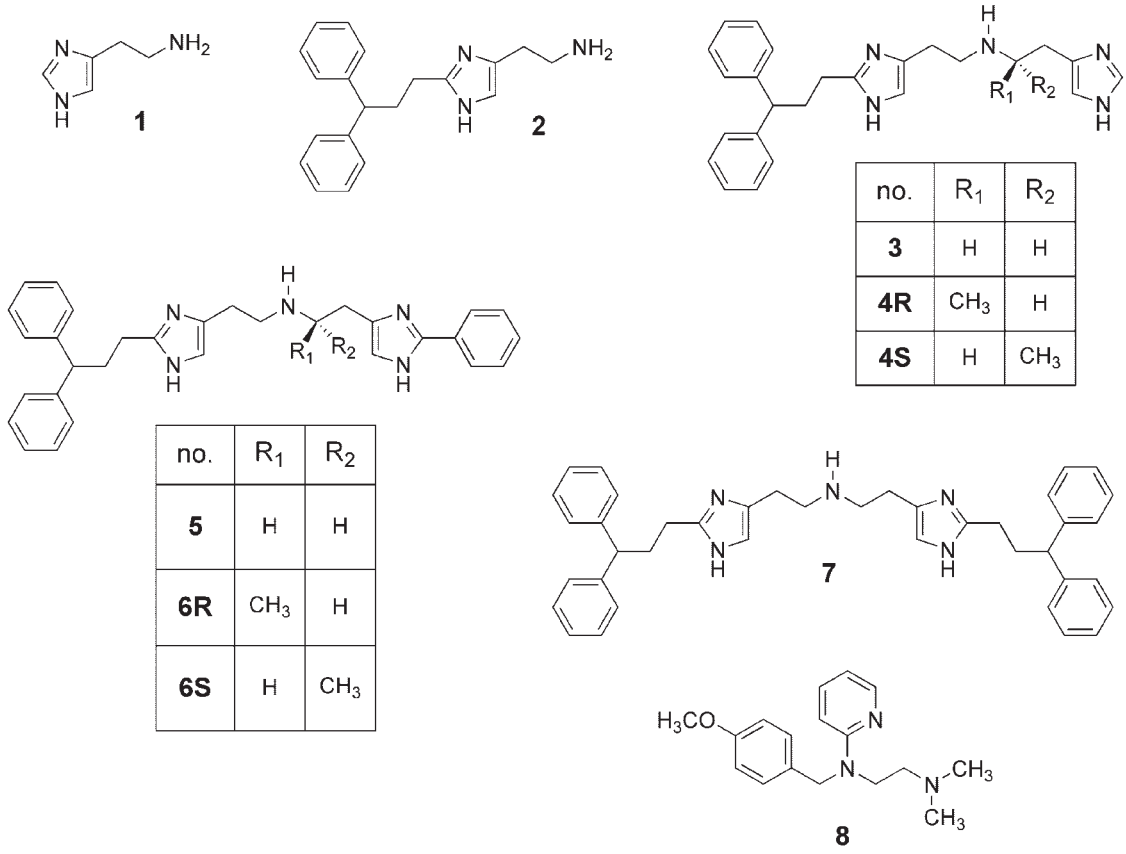

Fig. 1. Structures of histamine, histaprodifens, and mepyramine. Histamine **1**, histaprodifens **2** to **7**, and mepyramine **8**.

prodifen and suprahistaprodifen and participates in binding of large ligands by forming hydrogen bonds (Straßer et al., 2008). Furthermore, the N terminus presumably interacts with the E2-loop. Comparing the amino acid sequences of the N terminus and E2-loop between hH_1R and gpH_1R, species differences of approximately 60% for the N terminus and of approximately 30% for the E2-loop are found (Fig. 2).

Several studies have analyzed the contribution of the E2-loop to agonist or antagonist binding or activation of GPCRs, and the same analysis was performed with the adenosine A_1, A_{2a}, A_3 receptors (Olah et al., 1994; Kim et al., 1996), the dopamine D_2 receptor (Shi and Javitch, 2004), the muscarinic acetylcholine M_3 receptor (Scarselli et al., 2007), the α_1-adrenergic receptor (Zhao et al., 1996), the α_{2A}-adrenergic receptor (Laurila et al., 2007), and the histamine H_2 receptor (Preuss et al., 2007). To study the influence of the species differences in N terminus and E2-loop between hH_1R and gpH_1R, we constructed chimeric hH_1R with gp E2-loop ($h_{gpE2}H_1R$) and hH_1R with gp N terminus and gp E2-loop ($h_{gpNgpE2}H_1R$) (Fig. 3A). The wild-type and chimeric H_1Rs were coexpressed with the regulator of G protein signaling 4 (RGS4) in Sf9 insect cells. We characterized some histaprodifens (Fig. 1) in [^{3}H]mepyramine competition binding assay and GTPase assay. In addition, active-state models based on the crystal structure of bovine rhodopsin and β_2 receptor were constructed and compared to each other.

Materials and Methods

Materials. Phusion high-fidelity polymerase, all restriction enzymes, and T4 DNA ligase were obtained from New England Biolabs (Ipswich, MA). The anti-Flag IgG (M1 monoclonal antibody) was obtained from Sigma-Aldrich (St. Louis, MO), and the anti-RGS4 was from Santa Cruz Biotechnology, Inc. (Santa Cruz, CA). [γ-^{32}P]GTP was synthesized as described previously (Preuss et al., 2007), and [^{3}H]mepyramine (30.0 Ci/mmol) was obtained from PerkinElmer Life and Analytical Sciences (Waltham, MA). A Rotiszint ecoplus (Roth, Karlsruhe, Germany) liquid scintillation cocktail was used. Histaprodifens were synthesized as described by Elz et al. (2000), Menghin et al. (2003), and Striegl (2006).

Construction of $pGEMh_{gpE2}H_1R$, $pGEMh_{gpNgpE2}H_1R$, $pVLh_{gpE2}H_1R$, and $pVLh_{gpNgpE2}H_1R$. First, a pGEM-3*Z*-SF-$h_{gpN}H_1R$ plasmid was constructed. Therefore, pGEM-3*Z*-SF-gpH_1R-plasmid and pGEM-3*Z*-SF-hH_1R plasmid were double-digested with HindIII and PflMI, resulting in the fragments h-I, h-II, gp-I, and gp-II (Fig. 3B). The fragments h-I and gp-I were digested with PvuII, producing four fragments as follows: h-Ia, h-Ib, gp-Ia, and gp-Ib (Fig. 3B). Fragments h-Ia and gp-Ia encode parts of the pGEM-3*Z*-SF-plasmid, the N terminus, and the very beginning of transmembrane domain (TM) I. After separation and cleaning of the fragments, a triple ligation with gp-Ia, h-Ib, and h-II was performed. For generation of pGEM-3*Z*-SF-$h_{gpE2}H_1R$ and pGEM-3*Z*-SF-$h_{gpNgpE2}H_1R$, overlap-extension polymerase chain reactions (PCR) (PCR Ia, PCR Ib, and PCR II) with pGEM-3*Z*-SF-hH_1R and pGEM-3*Z*-SF-$h_{gpN}H_1R$ plasmid, respectively, as template were performed. In PCR Ia, the DNA fragment with the signal peptide (S), the FLAG epitope (F), and the first part of the $h_{gpN}H_1R$ up to transmembrane domain IV with guinea pig E2-loop was amplified. In PCR Ib, the DNA fragment encoding the guinea pig E2-loop, the second part of the hH_1R, and the His_6 tag (CACCATCATCACCATCAC) was generated. In PCR II, the products of PCR Ia and PCR Ib were annealed in the gp E2-loop-encoding region, resulting in PCR fragments that encode the SF, $h_{gpNgpE2}H_1R$, the His_6 tag, the stop codon, and an XbaI site. For PCRs, the following primers targeting the E2-loop were used:

```
          |----------N-Terminus----------||-------------TM1------------||-I1-||-------------
hH1R      MS-LPNSSCL--------LEDKMCEGNKTTMASPQLMPLVVVLSTICLVTVGLNLLVLYAVRSERKLHTVGNLYIVSLSVADL-74
gpH1R     ..F..GMTPVTLSNFSWA...R.L...S..TPTR....*....*.SVS....A.*.............................*.-83

          ---TM2---------||-E1-||---------------TM3---------------||----I2----||-------TM4-----
hH1R      IVGAVVMPMNILYLLMSKWSLGRPLCLFWLSMDYVASTASIFSVFILCIDRYRSVQQPLRYLKYRTKTRASATILGAWFLSFL-157
gpH1R     .........S...*HR.A.I.........*...*..*...*.........*............R..............*L....-166

          ------||---------E2---------||----------TM5-----------||---------------------------
hH1R      WVIPILGWNHFMQQTSVRREDKCETDFYDVTWFKVMTAIINFYLPTLLMLWFYAKIYKAVRQHCQHRELINRSLPSFSEIKLR-240
gpH1R     *.......H...AP..EP..K..*.....................*........IR......R.....Q...S.......M..K-249

          ----------------------------------------I3-----------------------------------------
hH1R      PENPKGDAKKPGKESPWEVLKRKPKDAGGGSVLKSPSQTPKEMKSPVVFSQEDDREVDKLYCFPLDIVHMQAAAEGSSRDYVA-323
gpH1R     L..A.V.TRRM.......DP..CSK..S.VHTPMPS..HLVD.PCAA.L.EDEGG..GTR--------Q.PML.V.DG.CCE.-324

          ------------------------------------------------------------------------------------
hH1R      VHMNRSHGQLKTDEQGLNTHGASEISEDQMLGDSQSFSRTDSDTTTETAPGKGKLRSGSNTGLDYIKFTWKRLRSHSRQYVSG-406
gpH1R     L.L.HMHS..ELSG.SRA..SI.ARP.EWTVV.G...PI.....S..A..MG.QP.....S..................T..-407

          --||-------------TM6-------------||-E3--||--------TM7--------||---C-Terminus----|
hH1R      LNRERKAAKQLGFIMAAFILCWIPYFIFFMVIAFCKNCCNEHLHMFTIWLGYINSTLNPLIYPLCNENFKKTFKRILHIRS-487
gpH1R     ............C.........*...*.V.........S.S..PV.....*....*L.....*..........R.......R.PP-488
```

Fig. 2. Alignment of the amino acid sequences of hH_1R and gpH_1R. The amino acid sequences are given in the one-letter code. Dots in the sequence of gpH_1R indicate amino acids that are identical to hH_1R. Hyphens indicate missing amino acids. Bold letters indicate glycosylation sites in the N terminus and E2-loop. Amino acids with gray shading are the most conserved amino acids (X.50, with X being the number of the TM domain), according to the numbering scheme in Ballesteros et al. (2001). Amino acids in white with black shading show the amino acids that are proposed to interact with the dimeric histaprodifen in the binding pocket of H_1R, based on the simulation results of the new model. Bold and underlined amino acids interact with dimeric histaprodifen in the binding pocket of H_1R only in the bovine rhodopsin-based model, but not in the $h\beta_2AR$-based model. The alignment was performed manually.

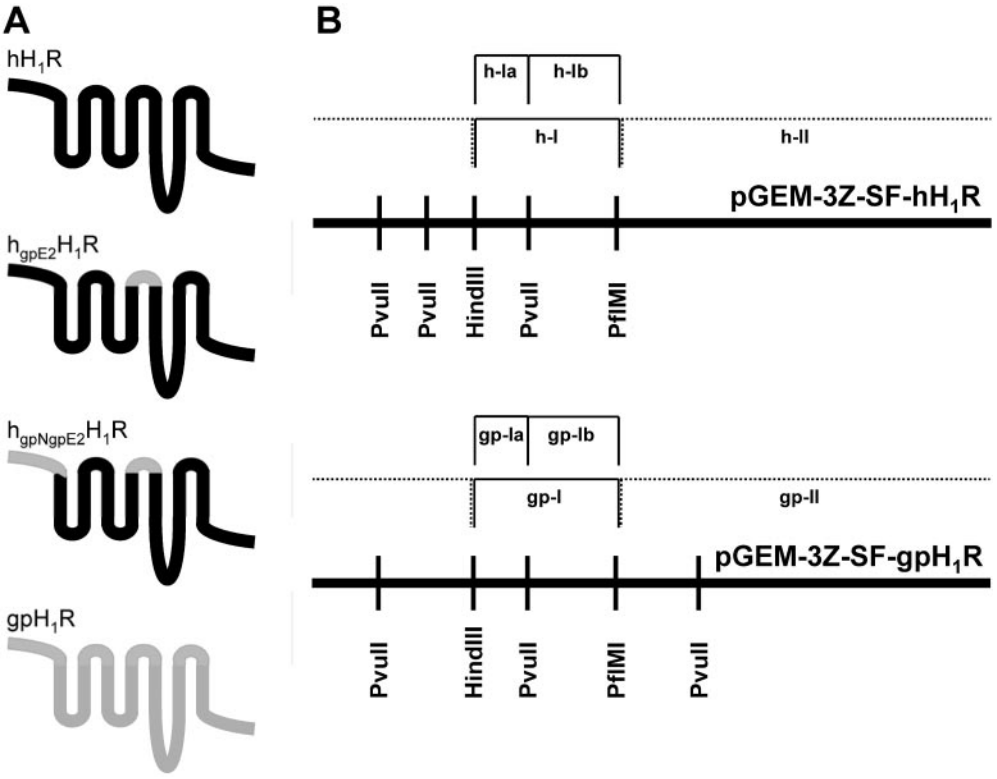

Fig. 3. Scheme of the wild-type hH_1R and gpH_1R and the chimeras $h_{gpE2}H_1R$, $h_{gpNgpE2}H_1R$, and fragments used for construction of $h_{gpE2}H_1R$. A, hH_1R, black; $h_{gpE2}H_1R$, the parts of hH_1R are given in black, and the E2-loop according gpH_1R is shown in gray; $h_{gpE2gpN}H_1R$, the parts of hH_1R are given in black, and the N terminus and E2-loop according gpH_1R are shown in gray; gpH_1R, gray. B, the sequence of pGEM-3Z-SF-hH_1R and pGEM-3Z-SF-gpH_1R with PvuII, HindIII, and PflMI sites is given schematically. The fragments resulting from digestion are marked.

GCTCACTCATTAGGCACC (forward, PCR Ia, PCR II); *TTTCTCCCGGGGCTCACTAGTCGGGGCCATGAAGTGGTG*CCAGCCTAGAATGGGAATAAC (reverse, PCR Ia); *CACCACTTCATGGCCCCGACTAGTGAGCCCCGGGAGAAA*AAGTGTGAGACAGACTTCTAT (forward, PCR Ib); and GGATCCTCTAGATTAGTGATGGTGATGATGGTG (reverse, PCR Ib, PCR II). The underlined code indicates a silent mutation for introduction of a unique diagnostic SpeI site. Italic letters designate the E2-loop. The resulting PCR fragment was double-digested with HindIII and XbaI and cloned into the pGEM-3Z plasmid using pGEM-3Z-SF gpH_1R as a template. The sequences of $h_{gpE2}H_1R$ and $h_{gpNgpE2}H_1R$, cloned into the pGEM-3Z-SF plasmid, were checked for their correctness by sequencing (Entelechon, Regensburg, Ger-

many). pGEM-3Z-SF-$h_{gpE2}H_1R$ and pGEM-3Z-SF-$h_{gpNgpE2}H_1R$ were used as a template to clone $h_{gpE2}H_1R$ and $h_{gpNgpE2}H_1R$ into the pVL1392 baculovirus transfer vector using the restriction sites BssHII and XbaI. All wild-type and chimeric H_1Rs were N-terminally tagged with the signal peptide and FLAG epitope ATGAAGACGATCATCGCCCTGAGCTACATCTTCTGCCTGGTATTCGCCGACTACAAGGACGATGATGACGCC and C-terminally tagged with the His_6 tag CACCATCATCACCATCAC.

Preparation of Compound Stock Solutions. Chemical structures of the analyzed compounds are given in Fig. 1. Compounds **1** and **8** (10 mM each) were dissolved in double-distilled water. Compounds **2** to **6** were dissolved in a solvent mixture containing 30% (v/v) dimethyl sulfoxide (DMSO), 30% (v/v) Tris-HCl, pH 7.4 (10 mM), and 40% (v/v) double-distilled water, 5 mM each. Compound **7** was dissolved in 50% (v/v) DMSO and 50% (v/v) Tris/HCl, pH 7.4 (10 mM), at a concentration of 1 mM. This lead to a 1:10 dilution of DMSO in each assay tube. Reference binding and GTPase assays with three preparations of histamine dissolved in 1) double-distilled water, 2) 30% (v/v) DMSO, 30% (v/v) Tris-HCl, pH 7.4 (10 mM), 40% (v/v) double-distilled water [equivalent to a final DMSO concentration of 3% (v/v)], and 3) 50% (v/v) DMSO, 50% (v/v) Tris-HCl, pH7.4 (10 mM), equivalent to a final DMSO concentration of 5% (v/v), respectively, revealed only a decrease in the radioactivity counted, but to no shift in pK_i and pEC_{50} values.

Miscellaneous. Cell culture, generation of recombinant baculoviruses, and membrane preparations were performed as described in Straßer et al. (2008). The determination of protein concentration, the SDS-polyacrylamide gel electrophoresis, and the immunoblot analysis were performed as described previously (Seifert et al., 2003; Straßer et al., 2008). The pharmacological assays, i.e., [^{3}H]mepyramine saturation binding assay, [^{3}H]mepyramine competition binding assay, and steady-state GTPase assay, were performed as described previously (Straßer et al., 2008). All assays for comparison of pharmacological data pharmacological data between the wild-type species isoforms of hH_1R and gpH_1R with the chimerics $h_{gpE2}H_1R$ and $h_{gpNgpE2}H_1R$ were carried out in parallel and under the same experimental conditions. All data were analyzed with Prism 4.02 (GraphPad Software Inc., San Diego, CA). pK_i and pK_B values were calculated according to the Cheng and Prusoff (1973) method. All data are the means ± S.E.M. of at least three independent experiments. To compare two pairs of data, the significance of the deviation of zero p was calculated using the t test.

Construction of Active H_1R Models with Dimeric Histaprodifen in the Binding Pocket. Besides the well known crystal structure of bovine rhodopsin, in recent studies, the crystal structure of an additional GPCR, namely the human β_2-adrenergic receptor ($h\beta_2AR$), was solved (Cherezov et al., 2007; Rasmussen et al., 2007; Rosenbaum et al., 2007). Therefore, two homology models of gpH_1R, based on the two different crystal structures, were generated. The generation of the gpH_1R model based on the crystal structure of bovine rhodopsin was described previously (Straßer and Wittmann, 2007). The gpH_1R homology model based on the crystal structure of the $h\beta_2AR$ (2RH1.pdb) (Cherezov et al., 2007; Rasmussen et al., 2007; Rosenbaum et al., 2007) was constructed in the same manner for all parts of the receptor, with the exception of the N terminus and E2-loop. Because of the lack of the conformation of the N terminus in the crystal structure of the $h\beta_2AR$, the N terminus was adopted from the crystal structure of bovine rhodopsin. The alignment of the E2-loop was performed manually and is given in Fig. 4. The modeling of the E2 regions His175 − Phe177, Ala179 − Pro184, and Glu190 − Tyr194 was performed using the loop-search module of the software SYBYL 7.0 (Tripos, St. Louis, MO). The helix structure of the E2-loop in the crystal structure of $h\beta_2AR$ was not implemented in the homology model of gpH_1R. In the crystal structure of the $h\beta_2AR$, two disulfide bridges, Cys191(E2) − Cys-184(E2) and Cys192(E2) − Cys106 (TM3, 3.25), are found. In the gpH_1R model, only one disulfide bridge, Cys189(E2) − Cys109(TM3, 3.25), is modeled. The resulting homology model was energetically minimized and embedded in an environment consisting of 1-palmitoyl-2-oleoyl-phosphatidylcholine molecules, intracellular and extracellular water molecules, sodium, and chloride ions. Molecular dynamics (MD) simulations to generate an active gpH_1R model based on the crystal structure of $h\beta_2R$ were performed in an analogous way as described previously (Straßer and Wittmann, 2007). In the active model, a positively charged dimeric histaprodifen was docked manually and after MD simulations were performed, as described previously (Straßer et al., 2008). Inactive and active models of hH_1R and $h_{gpNgpE2}H_1R$, based on the crystal structure of $h\beta_2AR$, were constructed in analogy to the corresponding gpH_1R model.

```
                    |----------------E2---------------|
bOPSD     174-GW-SRY-I--PEGMQC--S---CGIDYYTPHEETN-199
hb2AR     171--MHWYRATHQEAINCAYANETCC-DFF-T------196
hH1R      165--W-NHF-M--QQTSVR--REDKCETDFYD------186
gpH1R     174--W-HHF-M--APTSEP--REKKCETDFYD------195
```

Fig. 4. Alignment of the E2-loop of hH_1R and gpH_1R to the amino acid sequence of bovine rhodopsin and human β_2-adrenergic receptor. The cysteine forming a disulfide bridge to a cysteine residue in transmembrane domain III is shaded in gray. Hyphens indicate missing amino acids.

Based on the active-state models of the H_1Rs, additional MD simulations were carried out. The equilibration phase and the productive phase were performed as described previously (Straßer et al., 2008). For all calculations, the software package GROMACS 3.3.1 (van der Spoel et al., 2004) was used in combination with the ffG53A6 force field (Oostenbrink et al., 2004). The force-field parameters for dimeric histaprodifen **7** were adopted from the ffG53A6 force field.

Results

Immunological Detection of the H_1R Constructs. All H_1R constructs were immunologically detected with the M1 antibody (Fig. 5). hH_1R showed a strong band at ~85 kDa. In contrast, gpH_1R showed a strong band at 25 kDa, intermediate bands at ~30 and ~36 kDa, and faint bands at ~50 and ~100 kDa. For $h_{gpE2}H_1R$, a strong band was detected at ~60

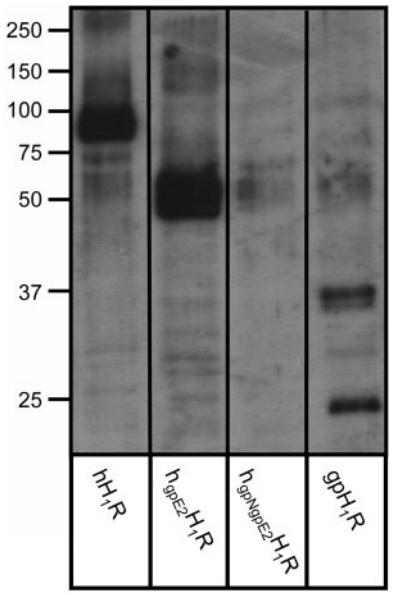

Fig. 5. Immunological detection of hH_1R, $h_{gpE2}H_1R$, $h_{gpNgpE2}H_1R$, and gpH_1R, expressed in Sf9 insect cell membranes. Sf9 cells, expressing one of the H_1Rs and RGS4, were analyzed in an immunoblot as described under *Materials and Methods*. For immunological detection, the M1 antibody was used. Each line represents one of the four analyzed H_1Rs. Numbers at the left indicate the apparent molecular masses of the proteins in kilodaltons.

kDa and weak bands were detected in a range from 25 to 37 kDa. For $h_{gpNgpE2}H_1R$, a weak band was visible at ~60 kDa, corresponding to $h_{gpE2}H_1R$. The ~60-kDa band of the chimeric constructs $h_{gpE2}H_1R$ and $h_{gpNgpE2}H_1R$ corresponds very well to the theoretical mass of ~56 kDa. The increase by 4 kDa relative to the theoretical mass is probably due to *N*-glycosylation. However, both chimeric constructs show different behavior with respect to the wild-type species isoforms, namely hH_1R and gpH_1R. These experimental results may be explained with different *N*-glycosylation states. At the N terminus, hH_1R exhibits two and gpH_1R exhibits one glycosylation site(s). Homology models of H_1Rs suggest that there is one additional *N*-glycosylation site for hH_1R in the E2-loop, but not for gpH_1R. Thus, hH_1R exhibits three ($h_{gpE2}H_1R$ two, $h_{gpNgpE2}H_1R$ one, and gpH_1R one) glycosylation site(s).

Analysis of the H_1R Wild-Type and Chimeric Species Isoforms in the [^{3}H]Mepyramine Saturation Binding Assay. The K_D and B_{max} values, which were determined in the [^{3}H]mepyramine saturation binding assay, are given in Table 1. There was no significant difference in the K_D values of hH_1R, $h_{gpE2}H_1R$, and $h_{gpNgpE2}H_1R$, which were 1.5 to 2-fold higher ($p < 0.05$) than at gpH_1R. The B_{max} value for $h_{gpE2}H_1R$ was in the same range as the value for hH_1R. The B_{max} value for $h_{gpNgpE2}H_1R$ was approximately 3-fold lower ($p < 0.05$) than that of $h_{gpE2}H_1R$, corresponding to the weaker immunoreactivity in the immunoblot (Fig. 5). The nonspecific binding of [^{3}H]mepyramine in Sf9 cells expressing wild-type and chimeric species isoforms was maximally 30%.

Analysis of Histaprodifens at H_1R Wild-Type and Chimeric Species Isoforms in the [^{3}H]Mepyramine Competition Binding Assay. The affinities of compounds **1** to **7**, determined in the competition binding assay, are given in Table 2. For compounds **1** to **4S** and **7**, no significant difference in pK_i values was found between hH_1R, $h_{gpE2}H_1R$, and $h_{gpNgpE2}H_1R$. However, for phenoprodifen **5** as well as for the chiral phenoprodifens **6R** and **6S**, a significant decrease in pK_i values was found in the series $hH_1R > h_{gpE2}H_1R \geq h_{gpNgpE2}H_1R$ (Fig. 6). For compound **5** at hH_1R, the pK_i value was significantly ($p < 0.005$) higher than at $h_{gpE2}H_1R$ and $h_{gpNgpE2}H_1R$. At hH_1R, the pK_i value of **6R** was significantly lower than that of **6S** ($p < 0.05$).

Constitutive Activity and Maximal Stimulation with Histamine of hH_1R, $h_{gpE2}H_1R$, $h_{gpNgpE2}H_1R$, and gpH_1R. The H_1R couples to endogenous G_q proteins of Sf9 insect cells (Houston et al., 2002). Agonist activation of the G_q proteins is detected by an increase of high-affinity GTP hydrolysis in membranes expressing H_1R and RGS proteins. The basal GTPase activity of the wild-type and chimeric H_1R species ranged from 1.1 to 1.5 pmol/(mg*min) without significant differences (Table 3). However, the maximal stimulation with 100 μM histamine **1** relative to the basal activity (ΔHA) at $h_{gpNgpE2}H_1R$ was significantly higher ($p < 0.005$) than at hH_1R, $h_{gpE2}H_1R$, and gpH_1R (Table 3). In addition, the ratio $\Delta HA/B_{max}$ was significantly higher ($p < 0.01$) at $h_{gpNgpE2}H_1R$ than at hH_1R, $h_{gpE2}H_1R$, and gpH_1R. Therefore, it can be concluded that the large stimulatory effect of histamine at $h_{gpNgpE2}H_1R$, despite the low expression level of $h_{gpNgpE2}H_1R$ in Sf9 cell membranes, is a consequence of receptor conformation due to binding of the endogenous ligand histamine **1**. The inverse agonist mepyramine **8** (Fitzsimons et al., 2004), which stabilizes the inactive state of the H_1R and consequently reduces constitutive activity (Seifert and Wenzel-Seifert, 2002), showed only small inhibitory effects on basal GTP hydrolysis at all four H_1Rs, indicating a low constitutive activity of the wild-type and chimeric H_1Rs (Table 3). The pEC_{50} values of mepyramine **8** ranged from 7.75 to 8.96 (Table 3). There was no significant difference between the pEC_{50} values of mepyramine between hH_1R and the chimeric H_1Rs, but the pEC_{50} values at the chimeric H_1Rs were significant lower ($p < 0.005$) than at gpH_1R.

Analysis of Histaprodifens at H_1R Wild-Type and Chimeric Species Isoforms in the Steady-State GTPase Assay. The potencies and efficacies (Table 4), and the pK_B values (Table 5), determined in the steady-state GTPase assay are given. A decrease in pEC_{50} values of histamine **1** in the series $hH_1R > h_{gpE2}H_1R > h_{gpNgpE2}H_1R$ was observed (Fig. 7). The potency of **1** at $h_{gpE2}H_1R$ and $h_{gpNgpE2}H_1R$ was significantly lower than hH_1R ($p < 0.05$ for $h_{gpE2}H_1R$ and $p < 0.005$ for $h_{gpNgpE2}H_1R$). For compounds **2** to **4S** and **7**, neither differences in potency nor efficacies were found between hH_1R and both chimeras. For the phenoprodifen **5**, a decrease in potency was found in the series $hH_1R > h_{gpE2}H_1R > h_{gpNgpE2}H_1R$. The chiral phenoprodifens **6R** and **6S** act as antagonists at $h_{gpE2}H_1R$ and $h_{gpNgpE2}H_1R$ as well as at hH_1R (Straßer et al., 2008). In accordance with the results in the competition binding (Fig. 6) assay, a decrease in pK_B values was found for **6R** as well as for **6S** in the series $hH_1R > h_{gpE2}H_1R > h_{gpNgpE2}H_1R$ (Table 4).

Binding Mode of Dimeric Histaprodifen in gpH_1R Models Based on Two Different Crystal Structures. The binding mode of dimeric histaprodifen **7** docked into the binding pocket of the gpH_1R active-state model, based on the crystal structure of bovine rhodopsin (Fig. 8A), was described in detail in Straßer et al. (2008). In comparison, the molecular dynamics simulations with dimeric histaprodifen **7** docked into the active-state model of the gpH_1R, based on the crystal structure of $h\beta_2AR$ (Fig. 8B), revealed some differences in the resulting binding mode. The largest difference between the two active gpH_1R models were found in the conformation and flexibility (Fig. 9) of the E2-loop. In the bovine rhodopsin-based gpH_1R model, the part of the E2-loop that shows species differences between hH_1R and gpH_1R is in close contact to the upper part of the binding pocket, near the transmembrane domain II. It is interesting to note that the backbone carbonyl of Lys187 (gpH_1R) forms a hydrogen bond to an imidazole moiety of dimeric histaprodifen. Because of a shift of the E2-loop in the $h\beta_2AR$-based model, Lys187 does

TABLE 1

[^{3}H]Mepyramine saturation binding in Sf9 cell membranes expressing hH_1R, $h_{gpE2}H_1R$, $h_{gpNgpE2}H_1R$, and gpH_1R with RGS4

Sf9 cell membranes coexpressing one of the H_1Rs and RGS4 were incubated with 0.2 to 20 nM [^{3}H]MEP as described under *Materials and Methods*. Nonspecific binding was determined in the presence of 10 μM diphenhydramine and was subtracted from total [^{3}H]MEP binding. The resulting binding data were analyzed by nonlinear regression and were best fitted to monophasic saturation curves. Data shown are the means ± S.E.M. of three independent membrane preparations, each one analyzed in triplicate.

	K_D	B_{max}
	nM	*pmol/mg*
hH_1R	4.49 ± 0.35	5.85 ± 1.67
$h_{gpE2}H_1R$	4.17 ± 0.75	3.91 ± 0.73
$h_{gpNgpE2}H_1R$	3.77 ± 0.67	1.90 ± 0.42
gpH_1R	2.53 ± 0.23	3.94 ± 0.83

TABLE 2

Affinities of histamine and histaprodifens at hH_1R, $h_{gpE2}H_1R$, $h_{gpNgpE2}H_1R$, and gpH_1R coexpressed with RGS4 in Sf9 cell membranes in the equilibrium competition binding assay

[^{3}H]MEP competition binding in Sf9 membranes expressing hH_1R, $h_{gpE2}H_1R$, $h_{gpNgpE2}H_1R$, and gpH_1R in combination with RGS4 was determined in presence of 5 nM [^{3}H]MEP as described under *Materials and Methods*. Data were analyzed by nonlinear regression and were best fit to one-site (monophasic) competition curves. The pK_i values were calculated according to the Cheng and Prusoff (1973) method. Data shown are the means ± S.E.M. of at least three experiments, each one performed in duplicate with independent membrane preparations.

Cpd	pK_i			
	hH_1R	$h_{gpE2}H_1R$	$h_{gpNgpE2}H_1R$	gpH_1R
1	5.62 ± 0.03	5.74 ± 0.04	5.75 ± 0.12	5.50 ± 0.03
2	6.47 ± 0.11	6.21 ± 0.08	6.06 ± 0.08	6.38 ± 0.11
3	6.33 ± 0.09	6.23 ± 0.03	6.29 ± 0.10	7.11 ± 0.10
4R	6.14 ± 0.07	5.96 ± 0.09	6.00 ± 0.07	6.94 ± 0.08
4S	5.40 ± 0.09	5.53 ± 0.08	5.58 ± 0.06	6.12 ± 0.08
5	6.60 ± 0.07	5.92 ± 0.04[a]	6.01 ± 0.02[a]	7.33 ± 0.08
6R	6.08 ± 0.06	5.94 ± 0.06[b]	5.72 ± 0.08[c]	6.74 ± 0.02
6S	6.40 ± 0.15	6.04 ± 0.11[b]	5.76 ± 0.04[c]	6.38 ± 0.17
7	6.67 ± 0.01	6.37 ± 0.08	6.58 ± 0.18	7.33 ± 0.14

[a] Comparison with pK_i at hH_1R, $p < 0.005$.
[b] Comparison with pK_i at hH_1R, $p < 0.05$.
[c] Comparison with pK_i at hH_1R, $p < 0.005$; comparison with pK_i at $h_{gpE2}H_1R$, $p < 0.05$.

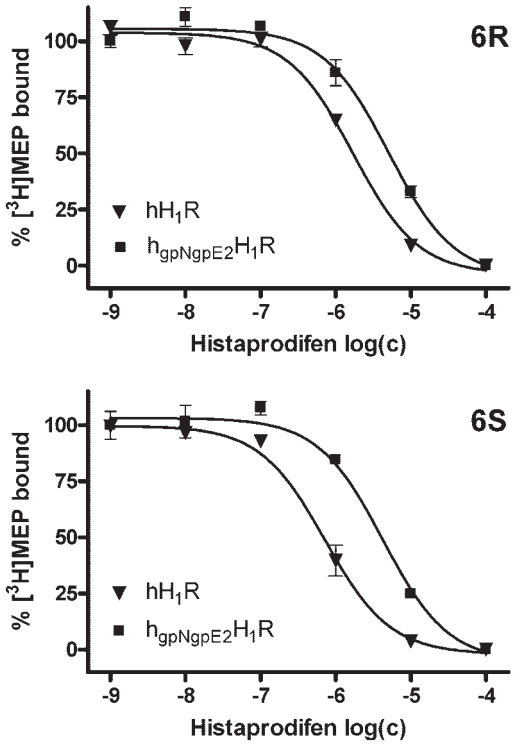

Fig. 6. Competition binding isotherms for **6R** and **6S** at hH_1R and $h_{gpNgpE2}H_1R$. The competition binding experiments were performed using Sf9 cell membranes expressing hH_1R or $h_{gpNgpE2}H_1R$ and RGS4 in the presence of 5 nM [^{3}H]mepyramine ([^{3}H]MEP) as described under *Materials and Methods*. Data were analyzed by nonlinear regression and were best fit to one-site (monophasic) competition curves. The downward-facing triangle (▼) shows the data for hH_1R, and the square (■) shows the data for the chimerical $h_{gpNgpE2}H_1R$. Data shown are the means ± S.E.M. of at least three experiments, each one performed in duplicate. Membranes were used from independent membrane preparations.

not interact with dimeric histaprodifen. The following amino acids were found to participate in the binding of **7** in the new model: Leu39 (TM1, 1.35), Leu43 (TM1, 1.39), Leu97 (TM2, 2.65), Trp112 (TM3, 3.28), Ile124 (TM3, 3.40), Trp429 (TM6, 6.48), and Trp456 (TM7, 7.40). The quaternary amine moiety in the center of **7** interacts electrostatically with the negatively charged Asp116 (TM3, 3.32) and Tyr459 (TM7, 7.43). One of the imidazole moieties forms stable hydrogen bonds with Ser120 (TM3, 3.36) and Tyr432 (TM6, 6.51). The second imidazole moiety forms stable hydrogen bonds to Glu190 (E2-loop) and Trp456 (TM7, 7.40) (Fig. 8). Both dipenyl propyl moieties of the dimeric histaprodifen are embedded in hydrophobic pockets.

The conserved disulfide bond between two cysteine side chains in TM3 and the E2-loop is responsible for a reduced flexibility in this region of the E2-loop (Fig. 9). However, although molecular dynamic simulations show a high flexibility of the nonrestricted parts of the E2-loop, a movement toward the binding pocket is notably observed. The interaction between the conserved Glu and the ligand is observed only in cases where the E2-loop is close to the binding pocket. This hydrogen bond stabilizes the conformation of the ligand in the binding pocket and reduces the flexibility of the ligand. The exchange of N terminus and E2-loop exerted an influence onto the hydrogen bond network between N terminus, E1-loop, and E2-loop with an effect on E2-loop conformation and flexibility (Fig. 9).

Discussion

GTPase Activation and Potency of Histamine at the Chimeric $h_{gpNgpE2}H_1R$ Compared with hH_1R. Our steady-state GTPase assay data show that the double-chimeric $h_{gpNgpE2}H_1R$ has influence on the maximal G_q-protein stimulation with histamine and potency of histamine, compared with hH_1R. Because the single-chimeric $h_{gpE2}H_1R$ showed no influence on the maximal G_q-protein stimulation with histamine compared with hH_1R, it can be concluded that the N terminus or the N terminus in combination with the E2-loop is responsible for this observation. Molecular dynamics simulations revealed that the exchange of N terminus and E2-loop has an influence on the hydrogen bond network between N terminus, E1-loop, and E2-loop with an effect on the conformation and flexibility of the E2-loop. Based on these data, it can be concluded that the interaction of the N terminus with the extracellular parts of the receptor induces subtle long-range conformational changes, resulting in a larger stimulatory effect of histamine and a decreased potency at $h_{gpNgpE2}H_1R$ compared with hH_1R.

Influence of the N Terminus and E2-Loop on Pharmacological Differences of Histaprodifens between hH_1R and gpH_1R. The experimental data show that the chimeric

TABLE 3

Analysis of the effects of histamine and mepyramine and determination of the constitutive activity of hH_1R, $h_{gpE2}H_1R$, $h_{gpNgpE2}H_1R$, and gpH_1R in the steady-state GTPase assay

Sf9 cell membranes expressing hH_1R, $h_{gpE2}H_1R$, $h_{gpNgpE2}H_1R$, or gpH_1R in combination with RGS4 were used to study the constitutive activity. GTPase assays were performed as described under *Materials and Methods*. The concentration-response curves of the inverse agonist MEP (**8**) were determined in a concentration range from 0.1 to 10 μM. Data were analyzed by nonlinear regression and were best fit to sigmoidal concentration-response curves. The efficacy of histamine was set 1.00. The ΔHA value refers to the difference of maximal stimulation with 100 μM histamine relative to basal activity. The coefficient $\Delta HA/B_{max}$ was calculated based on the data given for ΔHA in this table and B_{max} values in Table 1. The ΔMEP value refers to the difference of basal activity relative to GTP hydrolysis in presence of 10 μM MEP. The relative effect of MEP in the last column is the percentage effect of MEP relative to HA. Data shown are means ± S.E.M. of three experiments, each one performed in duplicate.

	pEC_{50} (MEP)	ΔHA	$\Delta HA/B_{max}$	ΔMEP	Relative Effect. of MEP
		pmol/(mg/min)	*1/min*	*pmol/(m/min)*	
hH_1R	8.24 ± 0.26	2.17 ± 0.38	0.37 ± 0.17	0.11 ± 0.01	5.1 ± 0.1
$h_{gpE2}H_1R$	7.75 ± 0.21	2.41 ± 0.21	0.62 ± 0.17	0.07 ± 0.01	5.7 ± 0.1
$h_{gpNgpE2}H_1R$	7.92 ± 0.27	4.06 ± 0.29	2.13 ± 0.63	0.21 ± 0.02	5.4 ± 0.6
gpH_1R	8.96 ± 0.18	1.89 ± 0.26	0.48 ± 0.17	0.26 ± 0.03	13.8 ± 0.9

TABLE 4

Potencies and efficacies of histamine and histaprodifens at hH_1R, $h_{gpE2}H_1R$, $h_{gpNgpE2}H_1R$, and gpH_1R coexpressed with RGS4 in Sf9 cell membranes in the steady-state GTPase assay.

All GTPase experiments were performed as described under *Materials and Methods*. Data were analyzed by nonlinear regression and were best fit to sigmoidal concentration-response curves. The efficacy (E_{max}) of histamine was set 1.00. The E_{max} values of all other compounds were referred to this value. Data shown are means ± S.E.M. of at least three experiments, each one performed in duplicate or triplicate. Membranes were used from independent membrane preparations. The effects of **4S**, **6R**, and **6S** at hH_1R, $h_{gpE2}H_1R$, and $h_{gpNgpE2}H_1R$ were too small to determine pEC_{50} values. Therefore, E_{max} values were determined using ligand concentrations of 10 or 100 μM each.

Cpd	hH_1R		$h_{gpE2}H_1R$		$h_{gpNgpE2}H_1R$		gpH_1R	
	pEC_{50}	E_{max}	pEC_{50}	E_{max}	pEC_{50}	E_{max}	pEC_{50}	E_{max}
1	6.92 ± 0.07	1.00	6.65 ± 0.11[a]	1.00	6.51 ± 0.05[b]	1.00	6.69 ± 0.10	1.00
2	6.95 ± 0.06	0.62 ± 0.07	6.91 ± 0.12	0.59 ± 0.01	6.96 ± 0.08	0.61 ± 0.07	7.50 ± 0.09	0.74 ± 0.04
3	6.62 ± 0.19	0.84 ± 0.08	6.51 ± 0.11	0.82 ± 0.07	6.66 ± 0.13	0.83 ± 0.03	7.30 ± 0.18	0.89 ± 0.09
4R	6.65 ± 0.16	0.47 ± 0.16	6.80 ± 0.12	0.37 ± 0.03	6.50 ± 0.09	0.36 ± 0.03	7.35 ± 0.19	0.91 ± 0.03
4S	N.D.	0.02 ± 0.06	N.D.	0.07 ± 0.04	N.D.	0.07 ± 0.05	6.84 ± 0.13	0.71 ± 0.06
5	6.67 ± 0.08	0.52 ± 0.05	6.58 ± 0.05[c]	0.42 ± 0.08	6.43 ± 0.02[d]	0.61 ± 0.03	7.25 ± 0.16	0.79 ± 0.05
6R	N.D.	0.05 ± 0.05	N.D.	0.07 ± 0.05	N.D.	0.06 ± 0.04	7.20 ± 0.22	0.60 ± 0.10
6S	N.D.	0.04 ± 0.05	N.D.	0.03 ± 0.02	N.D.	0.02 ± 0.02	7.09 ± 0.09	0.23 ± 0.03
7	6.18 ± 0.12	0.65 ± 0.11	6.05 ± 0.04	0.60 ± 0.10	6.04 ± 0.08	0.60 ± 0.05	7.18 ± 0.18	0.92 ± 0.08

N.D., not determined.
[a] Comparison with pEC_{50} at hH_1R, $p < 0.05$.
[b] Comparison with pEC_{50} at hH_1R, $p < 0.005$; comparison with pEC_{50} at $h_{gpE2}H_1R$, no significant difference.
[c] Comparison with pEC_{50} at hH_1R, no significant difference.
[d] Comparison with pEC_{50} at hH_1R, $p < 0.05$; comparison with pEC_{50} at $h_{gpE2}H_1R$, $p < 0.05$.

TABLE 5

Potencies of histaprodifens acting as antagonists at hH_1R, $h_{gpE2}H_1R$, and $h_{gpNgpE2}H_1R$ determined in the steady-state GTPase assay at Sf9 cell membranes expressing hH_1R, $h_{gpE2}H_1R$, or $h_{gpNgpE2}H_1R$, and RGS4

The potencies of **4S**, **6R**, and **6S** were determined in the steady-state GTPase assay as described under *Materials and Methods*. Each assay tube additionally contained 1 μM histamine. Data were analyzed by nonlinear regression and were best fit to sigmoidal concentration-response curves. The pK_B values were calculated according to Cheng and Prusoff (1973) method. Data shown are means ± S.E.M. of at least three experiments, each one performed in duplicate or triplicate. Membranes were used from independent membrane preparations.

Cpd	pK_B		
	hH_1R	$h_{gpE2}H_1R$	$h_{gpNgpE2}H_1R$
4S	6.00 ± 0.11	6.07 ± 0.22	5.80 ± 0.07
6R	6.56 ± 0.15	6.07 ± 0.11	5.55 ± 0.01
6S	6.61 ± 0.11	6.16 ± 0.16	5.98 ± 0.14

$h_{gpE2}H_1R$ and $h_{gpNgpE2}H_1R$ are well expressed in Sf9 cell membranes and show full functionality. However, the pharmacological studies specifically binding assays and steady-state GTPase assays indicate that the N terminus and the E2-loop are not responsible for the species differences between hH_1R and gpH_1R with regard to pK_i, pEC_{50}, and E_{max} values for compounds **2** to **4S** and **7**. Nevertheless, for the three phenoprodifens (**5**, **6R**, and **6S**) with a high structural similarity, a significant decrease in pK_i and pEC_{50} values was found in the series $hH_1R > h_{gpE2}H_1R > h_{gpNgpE2}H_1R$.

Our molecular dynamics simulations with the new gpH_1R model, based on the crystal structure of $h\beta_2AR$, show that the backbone carbonyl of Lys187 (gpH_1R) is far away from the binding pocket and does not interact with a large histaprodifen in the binding pocket, as suggested by the gpH_1R model based on the crystal structure of bovine rhodopsin. In addition, the molecular dynamic simulations based on the $h\beta_2AR$ model show that the highly conserved Glu181 (hH_1R) and Glu190 (gpH_1R), respectively, within the H_1R family point toward the binding pocket with formation of a stable hydrogen bond to the ligand and point away from the binding pocket forming a stable hydrogen bond to Tyr96 (TM2, 2.42). The MD simulations have shown that the exchange of the N terminus and E2-loop exhibits an influence of the hydrogen bond network in the extracellular part of the receptor with an effect on E2-loop conformation and flexibility, which results in decreased pK_i and pK_B values for the phenoprodifens **5**, **6R**, and **6S** at the chimeric H_1Rs. Furthermore, we assume that **5**, **6R**, and **6S** can bind in two different orientations into the binding pocket (Straßer et al., 2008). It is possible that a change in orientation of **5**, **6R**, and **6S** in the series $hH_1R - h_{gpE2}H_1R - h_{gpNgpE2}H_1R$ can explain our experimental data. Because the largest differences between hH_1R, the chimeric H_1Rs, and gpH_1R occur in the extracellular surface of the receptor, it is assumed that this possible change in orientation is determined kinetically during the early steps of the ligand binding process. To test this hypothesis, sophisticated kinetic binding studies have to be carried out. Furthermore, extensive molecular dynamics simulations with compounds

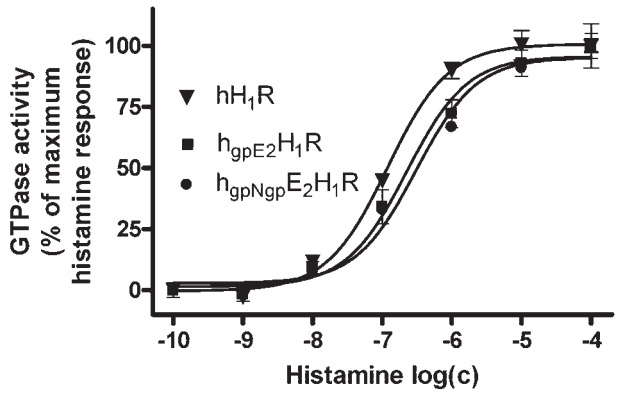

Fig. 7. Concentration-response curves for histamine **1** at hH_1R, $h_{gpE2}H_1R$, and $h_{gpNgpE2}H_1R$ in the steady-state GTPase assay. The experiments were performed using Sf9 cell membranes coexpressing hH_1R, $h_{gpE2}H_1R$, or $h_{gpNgpE2}H_1R$ and RGS4 as described under *Materials and Methods*. The downward-facing triangle (▼) shows the data for hH_1R, and the square (■) shows the data for the chimerical $h_{gpNgpE2}H_1R$. Data shown are the means ± S.E.M. of at least three experiments, each one performed in duplicate with independent membrane preparations.

5, **6R**, and **6S** at wild-type and chimeric H_1Rs are required to quantify the question of orientation.

Our new H_1R models indicate that the region of the E2-loop with species differences in amino acid sequence is pointing away from the binding pocket. It is possible that highly conserved amino acids in the E2-loop of H_1Rs are involved in ligand binding, e.g., Glu190 (E2-loop, gpH_1R), which shows electrostatic interaction with dimeric histaprodifen in the old gpH_1R model as well as in the new model. Additional experimental studies will be carried out to analyze the participation of Glu190 (E2-loop, gpH_1R) in binding of large histaprodifens.

Role of the Extracellular Loop E2 in Ligand Binding and Activation of GPCRs. Compared with other GPCR regions, relatively little attention has been paid thus far to the contribution of the second extracellular loop E2 in ligand recognition and ligand binding in biogenic amine and nucleoside GPCRs. Glutamate residues in the E2-loop of the human A_{2a} adenosine receptor are indirectly or directly involved in ligand binding (Kim et al., 1996). For the α_1-adrenergic receptor, amino acids, located in the extracellular loop E2, play a role in subtype-selective antagonist binding (Zhao et al., 1996). In addition, the affinity of yohimbine to the α_{2A}-adrenergic receptor is significantly influenced by interactions with the extracellular loop E2 (Laurila et al., 2007). Moreover, specific residues of the E2-loop are directly involved in forming the binding pocket of the dopamine D_2 receptor (Shi and Javitch, 2004). For the muscarinic M_3 receptor, several amino acids in the E2-loop are important for efficient agonist-induced activation of the muscarinic M_3 receptor (Scarselli et al., 2007). In contrast to these results, the E2-loop does not contribute to the species selectivity of guanidine-type agonists at human and guinea pig histamine H_2 receptor (Preuss et al., 2007). Our present study shows that the E2-loop and the E2-loop in combination with the N terminus have ligand-specific influence on the pharmacology of the H_1R. Based on these data, it can be concluded that the extracellular loop E2 as well as the N terminus contribute to ligand binding, receptor activation, and selectivity in biogenic amine and nucleoside GPCRs. Therefore, it seems to be

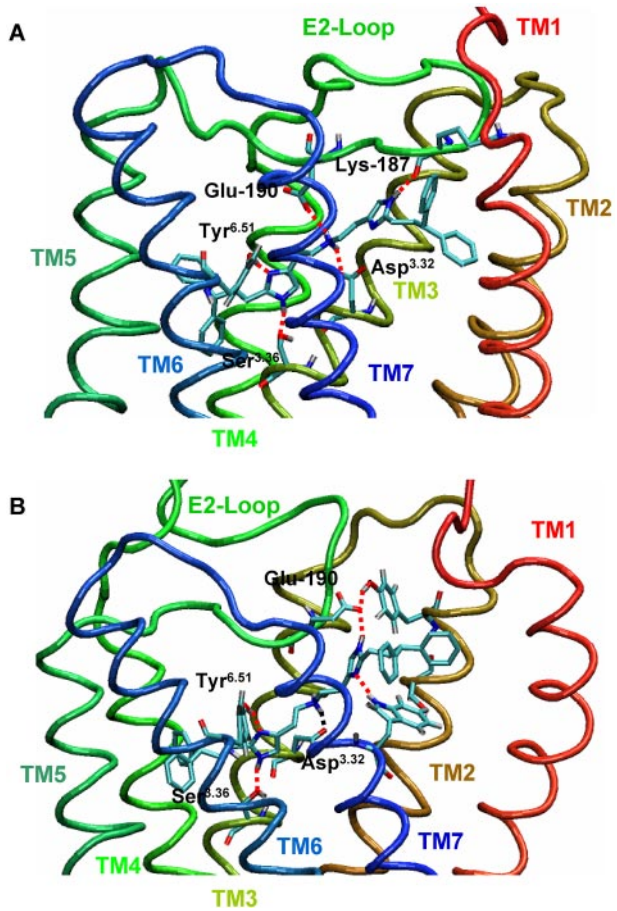

Fig. 8. Binding mode of dimeric histaprodifen **7** in the active gpH_1R model. Snapshot of dimeric histaprodifen **7** in the binding pocket of the active gpH_1R model during MD simulation. A, model based on the crystal structure of bovine rhodopsin. B, model based on the crystal structure of the $h\beta_2AR$. MD simulations were performed as described under *Materials and Methods*. Hydrogen bonds and electrostatic interactions between ligand and amino acids are marked as red dashed lines.

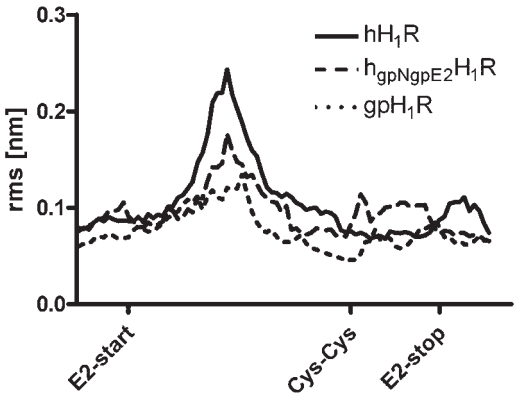

Fig. 9. Root mean square (rms) fluctuation of the backbone atoms of the E2-loop. The label Cys-Cys indicates the position of the disulfide bridge between E2-loop and TM3. This part of the E2-loop, which shows large species differences and is in no contact with the binding pocket, exhibits a decrease in backbone fluctuation within the series $hH_1R > h_{gpNgpE2}H_1R > gpH_1R$ (region between the labels E2-start and Cys-Cys). The region of the E2-loop with no species differences and contact to the ligand in the binding pocket shows a higher fluctuation for the $h_{gpNgpE2}H_1R$ compared with the wild-type H_1Rs. For all species, the fluctuation is reduced in the region of the disulfide bridge (Cys-Cys). All calculations were performed with GROMACS 3.3.1.

worthwhile to study the influence of N terminus and E2-loop on pharmacology and functionality of GPCRs in more detail.

Conclusion

Our studies have shown that the N terminus and E2-loop have ligand-specific influence onto the pharmacology of the H_1R. For a new class of histaprodifens, the phenoprodifens **5**, **6R**, and **6S** and the pK_i and pEC_{50} values (determined at hH_1R and the chimeric $h_{gpE2}H_1R$ and $h_{gpNgpE2}H_1R$) are not increased in direction of the gpH_1R but decreased to the contrary direction. Thus, despite the decrease in species differences in the amino acid sequence between hH_1R and gpH_1R, in the series $hH_1R \rightarrow h_{gpE2}H_1R \rightarrow h_{gpNgpE2}H_1R \rightarrow gpH_1R$, the differences in pharmacology increased for the phenoprodifens.

Acknowledgments

We thank Dr. S. Elz (Department of Pharmaceutical and Medicinal Chemistry I, University of Regensburg, Germany) for helpful discussions and support; K. Wohlfahrt for performing the molecular biological experiments and GTPase and binding assays; C. Huber for performing GTPase and binding assays; A. Seefeld for performing GTPase assays; and G. Wilberg for cell culture and immunoblot analysis.

References

Ballesteros JA, Shi L, and Javitch JA (2001) Structural mimicry in G protein-coupled receptors: implications of the high-resolution structure of rhodopsin for structure-function analysis of rhodopsin-like receptors. *Mol Pharmacol* **60:**1–19.

Bruysters M, Pertz HH, Teunissen A, Bakker RA, Gillard M, Chatelain P, Schunack W, Timmerman H, and Leurs R (2004) Mutational analysis of the histamine H_1-receptor binding pocket of histaprodifens. *Eur J Pharmacol* **487:**55–63.

Bruysters M, Jongejan A, Gillard M, van de Manakker F, Bakker RA, Chatelain P, and Leurs R (2005) Pharmacological differences between human and guinea pig histamine H_1 receptors: Asn^{84} (2.61) as a key residue within an additional binding pocket in the H_1 receptor. *Mol Pharmacol* **67:**1045–1052.

Cheng Y and Prusoff WH (1973) Relationship between the inhibition constant (K_i) and the concentration of inhibitor which causes 50 per cent inhibition (I_{50}) of an enzymatic reaction. *Biochem Pharmacol* **22:**3099–3108.

Cherezov V, Rosenbaum DM, Hanson MA, Rasmussen SG, Thian FS, Kobilka TS, Choi HJ, Kuhn P, Weis WI, Kobilka BK, et al. (2007) High-resolution crystal structure of an engineered human β_2-adrenergic G protein-coupled receptor. *Science* **318:**1258–1265.

Elz S, Kramer K, Pertz HH, Detert H, ter Laak AM, Kühne R, and Schunack W (2000) Histaprodifens: synthesis, pharmacological in vitro evaluation, and molecular modeling of a new class of highly active and selective histamine H_1-receptor agonists. *J Med Chem* **43:**1071–1084.

Fitzsimons CP, Monczor F, Fernández N, Shayo C, and Davio C (2004) Mepyramine, a histamine H_1 receptor inverse agonist, binds preferentially to a G protein coupled form of the receptor and sequesters G protein. *J Biol Chem* **279:**34431–34439.

Foord SM, Bonner TI, Neubig RR, Rosser EM, Pin JP, Davenport AP, Spedding M, and Harmar AJ (2005) International Union of Pharmacology. XLVI. G protein-coupled receptor list. *Pharmacol Rev* **57:**279–288.

Gillard M, Van Der Perren C, Moguilevsky N, Massingham R, and Chatelain P (2002) Binding characteristics of cetirizine and levocetirizine to human H_1 histamine receptor: contribution of Lys^{191} and Thr^{194}. *Mol Pharmacol* **61:**391–399.

Hill SJ, Ganellin CR, Timmerman H, Schwartz JC, Shankley NP, Young JM, Schunack W, Levi R, and Haas HL (1997) International Union of Pharmacology. XIII. Classification of histamine receptors. *Pharmacol Rev* **49:**253–278.

Houston C, Wenzel-Seifert K, Bürckstümmer T, and Seifert R (2002) The human histamine H_2-receptor couples more efficiently to Sf9 insect cell G_s-proteins than to insect cell G_q-proteins: limitations of Sf9 cells for the analysis of receptor/G_q-protein coupling. *J Neurochem* **80:**678–696.

Jongejan A and Leurs R (2005) Delineation of receptor-ligand interactions at the human histamine H_1 receptor by a combined approach of site-directed mutagenesis and computational techniques - or - how to bind the H_1 receptor. *Arch Pharm (Weinheim)* **338:**248–259.

Kim J, Jiang Q, Glashofer M, Yehle S, Wess J, and Jacobson KA (1996) Glutamate residues in the second extracellular loop of the human A2a adenosine receptor are required for ligand recognition. *Mol Pharmacol* **49:**683–691.

Kristiansen K (2004) Molecular mechanisms of ligand binding, signaling, and regulation within the superfamily of G-protein-coupled receptors: molecular modeling and mutagenesis approaches to receptor structure and function. *Pharmacol Ther* **103:**21–80.

Laurila JM, Xhaard H, Ruuskanen JO, Rantanen MJ, Karlsson HK, Johnson MS, and Scheinin M (2007) The second extracellular loop of α_{2A}-adrenoceptors contributes to the binding of yohimbine analogues. *Br J Pharmacol* **151:**1293–1304.

Leurs R, Smit MJ, Tensen CP, Ter Laak AM, and Timmerman H (1994) Site-directed mutagenesis of the histamine H_1-receptor reveals a selective interaction of $asparagine^{207}$ with subclasses of H_1-receptor agonists. *Biochem Biophys Res Commun* **201:**295–301.

Leurs R, Smit MJ, Meeder R, Ter Laak AM, and Timmerman H (1995) Lysine200 located in the fifth transmembrane domain of the histamine H_1 receptor interacts with histamine but not with all H_1 agonists. *Biochem Biophys Res Commun* **214:**110–117.

Menghin S, Pertz HH, Kramer K, Seifert R, Schunack W, and Elz S (2003) N^{α}-Imidazolylalkyl and pyridylalkyl derivatives of histaprodifen: synthesis and in vitro evaluation of highly potent histamine H_1-receptor agonists. *J Med Chem* **46:**5458–5470.

Nonaka H, Otaki S, Ohshima E, Kono M, Kase H, Ohta K, Fukui H, and Ichimura M (1998) Unique binding pocket for KW-4679 in the histamine H_1 receptor. *Eur J Pharmacol* **345:**111–117.

Ohta K, Hayashi H, Mizuguchi H, Kagamiyama H, Fujimoto K, and Fukui H (1994) Site-directed mutagenesis of the histamine H_1 receptor: roles of aspartic $acid^{107}$, $asparagines^{198}$ and $threonine^{194}$. *Biochem Biophys Res Commun* **203:**1096–1101.

Olah ME, Jacobson KA, and Stiles GL (1994) Role of the second extracellular loop of adenosine receptors in agonist and antagonist binding. Analysis of chimeric A_1/A_3 adenosine receptors. *J Biol Chem* **269:**24692–24698.

Oostenbrink C, Villa A, Mark AE, and van Gunsteren WF (2004) A biomolecular force field based on the free enthalpy of hydration and solvation: the GROMOS force-field parameter sets 53A5 and 53A6. *J Comput Chem* **25:**1656–1676.

Preuss H, Ghorai P, Kraus A, Dove S, Buschauer A, and Seifert R (2007) Point mutations in the second extracellular loop of the histamine H_2 receptor do not affect the species-selective activity of guanidine-type agonists. *Naunyn Schmiedebergs Arch Pharmacol* **376:**253–264.

Rasmussen SGF, Choi HJ, Rosenbaum DM, Kobilka TS, Thian FS, Edwards PC, Burghammer M, Ratnala VRP, Sanishvili R, Fischetti RF, et al. (2007) Crystal structure of the human β_2 adrenergic G-protein-coupled receptor. *Nature* **450:**383–387.

Rosenbaum DM, Cherezov V, Hanson MA, Rasmussen SG, Thian FS, Kobilka TS, Choi HJ, Yao XJ, Weis WI, Stevens RC, et al. (2007) GPCR engineering yields high-resolution structural insights into β_2-adrenergic receptor function. *Science* **318:**1266–1273.

Scarselli M, Li B, Kim SK, and Wess J (2007) Multiple residues in the second extracellular loop are critical from M_3 muscarinic acetylcholine receptor activation. *J Biol Chem* **282:**7385–7396.

Seifert R and Wenzel-Seifert K (2002) Constitutive activity of G-protein-coupled receptors: cause of disease and common property of wild-type receptors. *Naunyn Schmiedebergs Arch Pharmacol* **366:**381–382.

Seifert R, Wenzel-Seifert K, Bürckstümmer T, Pertz HH, Schunack W, Dove S, Buschauer A, and Elz S (2003) Multiple differences in agonist and antagonist pharmacology between human and guinea pig histamine H_1-receptor. *J Pharmacol Exp Ther* **305:**1104–1115.

Shi L and Javitch JA (2002) The binding site of aminergic G protein-coupled receptors: the transmembrane segments and second extracellular loop. *Annu Rev Pharmacol Toxicol* **42:**437–467.

Shi L and Javitch JA (2004) The second extracellular loop of the dopamine D_2 receptor lines the binding-site crevice. *Proc Natl Acad Sci U S A* **101:**440–445.

Straßer A and Wittmann HJ (2007) Analysis of the activation mechanism of the guinea-pig Histamine H_1-receptor. *J Comput Aided Mol Des* **21:**499–509.

Straßer A, Striegl B, Wittmann HJ, and Seifert R (2008) Pharmacological profile of histaprodifens at four recombinant histamine H_1 receptor species isoforms. *J Pharmacol Exp Ther* **324:**60–71.

Striegl B (2006) *Synthese und funktionelle in-Vitro Pharmakologie neuer Histamin-H_1-Rezeptoragonisten aus der Suprahistaprodifen-Reihe.* Ph.D. dissertation, University of Regensburg, Regensburg, Germany.

van der Spoel D, Lindahl E, Hess B, van Buuren AR, Apol E, Meulenhoff PF, Tieleman DP, Sijbers ALTM, Feenstra KA, and van Drunen R, et al. (2004) *Gromacs,* Department of Biophysical Chemistry, University of Groningen, The Netherlands.

Wieland K, Ter Laak AM, Smit MJ, Kühne R, Timmerman H, and Leurs R (1999) Mutational analysis of the antagonist-binding site of the histamine H_1 receptor. *J Biol Chem* **274:**29994–30000.

Zhao MM, Hwa J, and Perez DM (1996) Identification of critical extracellular loop residues involved in α_1-adrenergic receptor subtype-selective antagonist binding. *Mol Pharmacol* **50:**1118–1126.

Address correspondence to: Dr. Andrea Straßer, Department of Pharmaceutical and Medicinal Chemistry I, University of Regensburg, Universitätsstraße 31, D-93053 Regensburg, Germany. E-mail: andrea.strasser@chemie.uni-regensburg.de